Received: 10 February 2023 | Revised: 22 December 2023 | Accepted: 1 April 2024

DOI: 10.1111/ejn.16362

RESEARCH REPORT

EJN European Journal of Neuroscience FENS WILEY

Examining iron-related off-target binding effects of ^{18}F-AV1451 PET in the cortex of Aβ+ individuals

Jason Langley[1] | **Ilana J. Bennett**[2] | **Xiaoping P. Hu**[1,3] | **for the Alzheimer's Disease Neuroimaging Initiative**

[1]Center for Advanced Neuroimaging, University of California Riverside, Riverside, California, USA

[2]Department of Psychology, University of California Riverside, Riverside, California, USA

[3]Department of Bioengineering, University of California Riverside, Riverside, California, USA

Correspondence
Xiaoping P. Hu, Ph.D., Provost Fellow, Professor and Chair Department of Bioengineering University of California, Riverside, Materials Science and Engineering 205, Riverside, CA, USA.
Email: xhu@engr.ucr.edu

Funding information
National Institutes of Health, Grant/Award Number: U01 AG024904; Department of Defense; National Institute on Aging; National Institute of Biomedical Imaging and Bioengineering; through generous contributions from the following: AbbVie, Alzheimer's Association; Alzheimer's Drug Discovery Foundation; Araclon Biotech; BioClinica, Inc.; Biogen; Bristol-Myers Squibb Company; CereSpir, Inc.; Cogstate; Eisai Inc.; Elan Pharmaceuticals, Inc.; Eli Lilly and Company; EuroImmun; F. Hoffmann-

Abstract

The presence of neurofibrillary tangles containing hyper-phosphorylated tau is a characteristic of Alzheimer's disease (AD) pathology. The positron emission tomography (PET) radioligand sensitive to tau neurofibrillary tangles (^{18}F-AV1451) also binds with iron. This off-target binding effect may be enhanced in older adults on the AD spectrum, particularly those with amyloid-positive biomarkers. Here, we examined group differences in ^{18}F-AV1451 PET after controlling for iron-sensitive measures from magnetic resonance imaging (MRI) and its relationships to tissue microstructure and cognition in 40 amyloid beta positive (Aβ+) individuals, 20 amyloid beta negative (Aβ-) with MCI and 31 Aβ- control participants. After controlling for iron, increased ^{18}F-AV1451 PET uptake was found in the temporal lobe and hippocampus of Aβ+ participants compared to Aβ- MCI and control participants. Within the Aβ+ group, significant correlations were seen between ^{18}F-AV1451 PET uptake and tissue microstructure and these correlations remained significant after controlling for iron. These findings indicate that off-target binding of iron to the ^{18}F-AV1451 ligand may not affect its sensitivity to Aβ status or cognition in early-stage AD.

KEYWORDS
Alzheimer's disease, MRI, PET, tau

Abbreviations: Aβ, amyloid beta; AD, Alzheimer's disease; ADAS, Alzheimer's Disease Assessment Scale; ADNI, Alzheimer's Disease Neuroimaging Initiative; ANCOVA, analysis of covariance; CDR, clinical dementia rating; DWI, Diffusion-weighted imaging; FA, fractional anisotropy; FSL, FMRIB software library; FLIRT, FMRIB's linear image registration tool; FNIRT, FMRIB's Nonlinear image registration tool; ICC, intraclass correlation coefficients; MCI, mild cognitive impairment; MD, mean diffusivity; MMSE, Mini-Mental State Examination; MNI, Montreal Neurological Institute; MOCA, Montreal cognitive assessment; MRI, magnetic resonance imaging; PET, positron emission tomography; PETPVC, PET partial volume correction; QSM, quantitative susceptibility mapping; ROI, region of interest; SUVR, standardized uptake value ratio.

Data used in preparation of this article were obtained from the Alzheimer's Disease Neuroimaging Initiative (ADNI) database (adni.loni.usc.edu). As such, the investigators within the ADNI contributed to the design and implementation of ADNI and/or provided data but did not participate in analysis or writing of this report. A complete listing of ADNI investigators can be found at http://adni.loni.usc.edu/wp-content/uploads/how_to_apply/ADNI_Acknowledgement_List.pdf.

La Roche Ltd and its affiliated company Genentech, Inc.; Fujirebio; GE Healthcare; IXICO Ltd.; Janssen Alzheimer Immunotherapy Research & Development, LLC.; Johnson & Johnson Pharmaceutical Research & Development LLC.; Lumosity; Lundbeck; Merck & Co., Inc.; Meso Scale Diagnostics, LLC.; NeuroRx Research; Neurotrack Technologies; Novartis Pharmaceuticals Corporation; Pfizer Inc.; Piramal Imaging; Servier; Takeda Pharmaceutical Company; and Transition Therapeutics; Canadian Institutes of Health Research; National Institutes of Health, Grant/Award Number: R01AG072607

Edited by: Susan Rossell

1 | INTRODUCTION

Alzheimer's disease (AD) is the most frequent cause of dementia and it is estimated that 1 in 85 people worldwide will develop AD by 2050 (Brookmeyer et al., 2007). Patients with mild cognitive impairment (MCI) exhibit declines in cognitive performance that do not meet the threshold for dementia, but are likely to later convert to AD (Albert et al., 2011). AD pathology is characterized by the presence of β-amyloid (Aβ) extracellular plaques and neurofibrillary tangles containing hyper-phosphorylated tau (Hardy & Allsop, 1991; Sayre et al., 2000; Selkoe, 1991). Both Aβ plaque and tau neurofibrillary tangle deposition precede cognitive decline (Arnsten et al., 2021; Braak et al., 2011; Hedden et al., 2013) and are associated with neurodegeneration and cognitive impairment (Bejanin et al., 2017; Gómez-Isla et al., 1997). Aβ pathology in individuals with MCI increases the risk of transitioning from MCI to dementia (Doraiswamy et al., 2012; Koivunen et al., 2011). In addition, Aβ pathology is related to higher rates of memory decline and higher rates of grey matter atrophy in cognitively normal elderly adults (Chételat et al., 2012; Lim et al., 2013).

The development of positron emission tomography (PET) radioligands sensitive to tau neurofibrillary tangles, such as ^{18}F-AV1451, has allowed for the visualization and assessment of AD pathology in vivo. Increased tau-PET uptake has been reported in individuals with AD relative to controls (Chen Jingyun et al., 2018; Cho et al., 2016; Johnson et al., 2016; Ossenkoppele et al., 2016; Passamonti et al., 2017; Whitwell et al., 2018) as well as in the medial temporal lobe of Aβ+ control participants relative to Aβ- control participants (Leuzy et al., 2022; Pascoal et al., 2021). Imaging studies using ^{18}F-AV1451 have found tau-PET signal to be associated with lower brain volume (Iaccarino et al., 2018) and cortical thickness (Gordon et al., 2018; Ossenkoppele et al., 2019; Xia et al., 2017) derived from T_1-weighted images. Other studies examining tissue microstructure measured using diffusion-weighted imaging, a MRI contrast sensitive to the motion of water molecules (Beaulieu, 2002), have found that tau-PET signal is also related to microstructure measures associated with neurodegeneration in AD (Lee et al., 2020; Sintini et al., 2019; Torso et al., 2021).

However, the radioligand used in ^{18}F-AV1451 binds with iron in addition to tau neurofibrillary tangles (Choi et al., 2018; Lockhart et al., 2017; Lowe et al., 2016; Marquié et al., 2017), which may confound these associations to cognition and tissue microstructure as changes in ^{18}F-AV1451 uptake could be due to iron or tau. In particular, strong associations in the cortex have been observed when tau-PET uptake is compared to tissue susceptibility (Cogswell et al., 2021; Spotorno et al., 2020), an MRI measure sensitive to iron (Langkammer et al., 2012). Elevated cortical iron levels have been observed in the AD spectrum (Ayton et al., 2015; Ayton et al., 2020; van Duijn et al., 2017; van Rooden et al., 2015). Further, imaging and histology studies have linked iron deposition to Aβ pathology (Connor et al., 1992; van Bergen et al., 2016), and cerebral amyloid angiopathy may contribute to iron deposition seen in the AD spectrum (Schrag et al., 2011). Taken together, this iron deposition may be related to altered uptake of the ^{18}F-AV1451 radioligand. To date, however, there has been a dearth of literature accounting for potential off-target binding of the ^{18}F-AV1451 radioligand on iron.

The current study sought to examine whether the previously reported relationships between ^{18}F-AV1451 tau-PET signal and tissue microstructure or cognitive impairment remain significant in the hippocampus and temporal lobe after controlling for iron, which would provide confidence that these relationships are in fact due to

tau and not iron. Multimodal neuroimaging analyses, combining iron-sensitive measures from MRI with ^{18}F-AV1451 PET, may allow for off-target binding effects of the ^{18}F-AV1451 radioligand to be assessed. We used tissue susceptibility as an independent marker for iron and examined effects before and after statistically controlling for this iron measure on ^{18}F-AV1451 PET uptake. Group differences in ^{18}F-AV1451 PET uptake and its relationship to tissue microstructure and cognition were examined in 40 Aβ+ individuals, 20 Aβ- with MCI and 31 Aβ- control participants.

2 | METHODS

2.1 | Alzheimer's disease neuroimaging initiative (ADNI) overview

Data used in this study were obtained from the ADNI database (adni.loni.usc.edu). ADNI was launched in 2003 as a public-private partnership-supported project. The primary goal of ADNI is to test whether serial MRI, PET, other biological markers and clinical and neuropsychological assessments can be combined to measure the progression of MCI and early AD. Up-to-date information can be found at www.adni-info.org. The ADNI data were collected from over 50 research sites and the ADNI study was approved by the local Institutional Review Boards (IRBs) of all participating sites. The detailed information and complete list of ADNI sites' IRBs could be found at https://adni.loni.usc.edu/about/centers-cores/study-sites/ and http://www.adni-info.org/.

Study participants and, if applicable, their legal representatives, gave written informed consent at the time of enrollment for imaging data, genetic sample collection and clinical questionnaires. Exclusion criteria determined by ADNI were followed. Participants were excluded from the analysis if they had Parkinson's disease, Huntington's disease, progressive supranuclear palsy, a history of seizures, normal pressure hydrocephalus, brain tumours, multiple sclerosis, subdural hematoma, a history of head trauma, known brain structural abnormalities, a history of major depression, schizophrenia, alcohol or substance abuse, bipolar disorder or currently using psychoactive medications. Individuals with contraindications to MRI imaging such as pacemakers, heart valves or other foreign objects or implants in the body were excluded.

2.2 | Participants

The ADNI3 database was queried for individuals with tau-sensitive PET (^{18}F-AV1451), multi-echo gradient echo MRI images and multi-shell diffusion-weighted MRI images at the same scanning visit, as well as Aβ status. From this cohort, we selected all individuals with a diagnostic status of MCI or control at the time of the visit, which included 40 Aβ positive (Aβ+) participants (20 Aβ + MCI and 20 Aβ+ controls), 20 Aβ negative (Aβ-) MCI participants and 31 Aβ- control participants. Imaging data were downloaded between December 2019 and July 2022.

All MCI participants in the ADNI3 database had a subjective memory concern reported by a clinician, abnormal memory function on the education-adjusted Logical Memory II subscale and a clinical dementia rating greater than 0.5. Further, MCI participants were deemed to have cognitive and functional performance that was sufficiently intact to not merit a diagnosis of attention deficit disorder by the site physician.

2.3 | MRI acquisition

All MRI data used in this study were acquired on Siemens Prisma or Prisma fit scanners. Anatomic images were acquired with an MP-RAGE sequence (echo time (TE)/repetition time (TR)/inversion time = 2.98/2300/900 ms, flip angle = 9°, voxel size = 1.0 × 1.0 × 1.0 mm^3 and GRAPPA acceleration factor = 2) and were used for registration to common space and correction of partial volume effects in the PET data.

Iron-sensitive data were collected with a three-echo 2D gradient recalled echo GRE) sequence ($TE_1/\Delta TE$/TR = 6/7/650 ms, flip angle = 20°, field of view = 220 × 220 mm^2, matrix size of 256 × 256, 44 slices, slice thickness = 4.0 mm) and used for measurement of brain iron.

Diffusion-weighted imaging (DWI) data were acquired with a multiband diffusion-weighted echo planar imaging (EPI) spin echo sequence (TE/TR = 71/3400 ms, field of view = 232 × 232 mm^2, voxel size = 2 × 2 × 2 mm^3, multiband acceleration factor = 3, PA phase encoding direction). Diffusion weighting was applied in 54 directions with b values of 1000 and 2000 s/mm^2. A two-echo 2D GRE sequence (TE_1/TE_2/TR = 4.92/7.38/571 ms, flip angle = 60°, voxel size = 3.0 × 3.0 × 3.0 mm^3) was used for correction of susceptibility distortion in the diffusion images.

2.3.1 | T_1-common space registration

Transforms for MRI imaging data were derived with FMRIB Software Library (FSL). A transformation was derived between individual subject space to 2 mm Montreal Neurological Institute (MNI) T_1-weighted space

using FMRIB's Linear Image Registration Tool (FLIRT) and FMRIB's Nonlinear Image Registration Tool (FNIRT) in the FSL software package using the following steps (Smith et al., 2004; Woolrich et al., 2009). First, the T_1-weighted image was skull-stripped using the brain extraction tool (BET). Next brain extracted T_1-weighted images were aligned with the MNI brain extracted image using an affine transformation. Finally, a nonlinear transformation was used to generate a transformation from individual T_1-weighted images to T_1-weighted MNI common space.

2.3.2 | QSM processing

Susceptibility images were constructed using the following procedure. First, a brain mask was derived from the first echo of the magnitude data. Next, the brain mask was carefully examined and any areas of the mask outside the brain were manually removed. The background phase was removed using harmonic phase removal using the Laplacian operator (iHARPERELLA) (Li et al., 2014). Finally, susceptibility maps were derived from the frequency map of brain tissue using an improved least-squares (iLSQR) method (Li et al., 2011; Li et al., 2015) and Laplace filtering with a threshold of 0.04 as a truncation value. All susceptibility images were processed in MATLAB (The MathWorks, Inc., Natick, MA, USA) using STISUITE. The resulting susceptibility maps were aligned to each subject's T_1-weighted image using a rigid body transform derived via the magnitude image from the first echo.

2.3.3 | DWI processing

Diffusion data were preprocessed with FSL (Jenkinson et al., 2002; Jenkinson & Smith, 2001; Smith et al., 2004) and were first corrected for motion and eddy currents using EDDY. Next, field maps were constructed and used to correct magnetic field inhomogeneities in the diffusion images using FUGUE. Finally, the $b = 0$ image was brain extracted and a transform between each subject's T_1-weighted and $b = 0$ images was derived using a rigid body transform with a boundary-based registration cost function.

Single-compartment parameters (fractional anisotropy, FA; mean diffusivity, MD) were derived from the diffusion data using DTIFIT. Advanced modelling was performed using the NODDI toolbox v1.0.1 (http://www.nitrc.org/projects/noddi_toolbox) in MATLAB (Zhang et al., 2012). NODDI fitting was performed using the default settings and maps of cerebrospinal fluid (CSF) volume fraction (denoted fiso) and the fraction of water in the restricted compartment (ficvf) were generated.

2.3.4 | PET acquisition and processing

The radiochemical synthesis of ^{18}F-AV1451 was overseen and regulated by Avid Radiopharmaceuticals and distributed to the qualifying ADNI sites where PET imaging was performed according to standardized protocols. The ^{18}F-AV-1451 protocol entailed the injection of 10 mCi of tracer followed by an uptake phase of 75 min during which the subjects remained out of the scanner, and then collection of the ^{18}F-AV-1451 emission data as 6 × 5 min frames. PET with computed tomography imaging (PET/CT) scans preceded these acquisitions with a CT scan for attenuation correction; PET-only scanners performed a transmission scan following the emission scan.

PET imaging data were analysed with FSL and PET partial volume correction (PETPVC) toolbox (Thomas et al., 2016). Motion was corrected in ^{18}F-AV1451 PET scans were co-registered to the first frame and averaged using rigid-body transforms with FLIRT in FSL. Next, the motion-corrected mean PET scans were registered to the participant's own T_1-weighted MRI image using a rigid-body transform with a normalized mutual information cost function in FLIRT. Grey matter, white matter and CSF maps were segmented in the T_1-weighted MRI image and used to correct for partial volume effects using PETPVC (Thomas et al., 2016). A combination of Labbé (Labbe et al., 1996) and region-based voxel-wise correction (Thomas et al., 2011) was chosen to mitigate sensitivity to point spread function mismatch. The median standardized uptake value (SUV) in the left + right cerebellar cortex was chosen as a reference. Figure 1 shows a

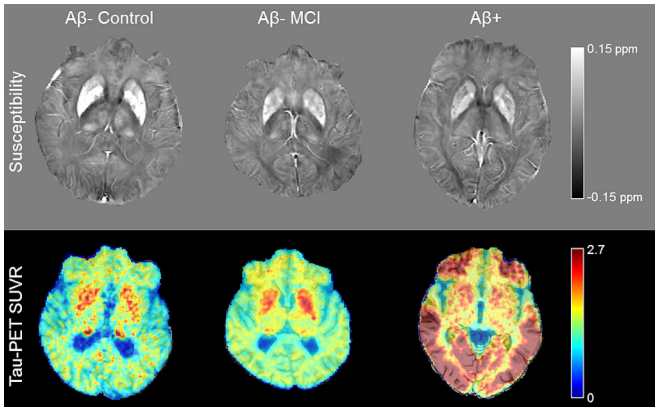

FIGURE 1 Illustrations of typical susceptibility (top row) and tau-PET SUVR (bottom row) images in subjects from the Aβ- control (left column), Aβ- MCI (middle column) and Aβ+ (right column) groups.

comparison of typical susceptibility maps and SUV ratios (SUVR) for a subject from each group.

2.4 | Regions of interest

Atlases from the Harvard-Oxford subcortical atlas and a prior study parcelling the cortex (Zhang et al., 2010) were used to define standard space regions of interest (ROIs) in the bilateral hippocampus and temporal lobe, respectively. The ROIs were then transformed from MNI space to subject space using linear and nonlinear transforms in FSL as described in the earlier sections.

Each aligned ROI was thresholded at 60% and binarized. To ensure that the signal from white matter did not contaminate measures in the temporal lobe, the binarized temporal lobe ROI was multiplied by each individual's grey matter mask. Mean single-compartment diffusion (FA, MD), NODDI (fiso, ficvf), tau-PET SUVR and susceptibility were measured in each resultant ROI for each participant.

2.5 | Statistical analysis

All statistical analyses were performed using IBM SPSS Statistics software version 24 (IBM Corporation, Somers, NY, USA) and results are reported as mean ± standard deviation. A P value of 0.05 was considered significant for all statistical tests performed in this work. Normality of tau-PET, diffusion and iron data was assessed using the Shapiro–Wilk test for each group and all data was found to be normal.

The effect of group (Aβ+, Aβ- MCI, Aβ-control) was tested with separate analysis of covariance (ANCOVA) in each ROI (hippocampus, temporal lobe) for each imaging metric (tau-PET SUVR, susceptibility, single compartment diffusion [FA, MD], multicompartment diffusion indices [fiso, ficvf]), controlling for sex and age. The ANCOVAs for tau-PET SUVR and single compartment diffusion metrics also controlled for susceptibility since iron is an off-target bind for the ^{18}F-AV1451 radioligand and local magnetic field inhomogeneities from iron produce cross terms with diffusion encoding gradients and reduce the apparent diffusion coefficient (Novikov et al., 2018; Zhong et al., 1991). This relationship between iron and single-compartment diffusion measures has been observed in vivo (Langley et al., 2020; Syka et al., 2015), but has not been observed for multicompartment diffusion measures (Langley et al., 2021). For all ANCOVAs, if the main effect of the group was significant, post hoc comparisons between each pair of groups were performed using respective two-tailed t-tests.

Iron-related off-target binding effects were assessed by examining the relationship between tau-PET SUVR and susceptibility using Pearson correlations in each ROI, separately for each group. The impact of iron on the relationship between tau-PET SUVR and both microstructural (FA, MD, fiso, ficvf) and cognitive (delayed word recall, ADAS13) measures was assessed by performing separate multiple regressions that excluded susceptibility as a predictor in the second step. For each dependent measure, an R^2-change F-test was used to statistically compare the models with and without controlling for susceptibility.

Scan-rescan reproducibility of cortical susceptibility was assessed using intraclass correlation coefficients (ICC) using control subjects with baseline and 12-month follow-up scans. Reproducibility of interscan cortical susceptibility measurements at baseline and 12-month follow-up was tested with a two-way random ICC evaluating absolute agreement. ICC is a measure of agreement between two groups of measurements and ICC values were interpreted according to the criteria set by Landis and Koch: $(0.8,1]$ = almost perfect agreement and $(0.6, 0.8]$ = substantial agreement (Landis & Koch, 1977).

3 | RESULTS

3.1 | Sample demographics

Demographic data for each group is shown in Table 1. Age exhibited a significant group effect with the Aβ + group having a higher age relative to the Aβ- control group ($P < 10^{-3}$) but no difference was observed in other group comparisons (Ps>0.115). As expected, significant group effects were observed in MOCA, MMSE and CDR, with the Aβ+ group and Aβ- MCI group showing lower scores on MOCA (Aβ+: $P < 10^{-3}$; Aβ-: $P = 0.003$) relative to the Aβ- control group, whereas only the Aβ+ group had a lower MMSE score than the control group ($P = 0.003$). Higher CDR (Aβ+:$P < 10^{-3}$; Aβ-: $P < 10^{-3}$) was observed in the Aβ+ group and Aβ- MCI group relative to the Aβ- control group. Significant group effects were also seen in ADAS delayed recall and ADAS13, with higher scores in the Aβ+ group relative to the Aβ- MCI (Ps<0.036) and control (Ps<10^{-3}) groups, and in the Aβ- MCI group relative to the control group (Ps<10^{-3}).

3.1.1 | Reproducibility of cortical susceptibility measurements

The reproducibility of mean cortical susceptibility was assessed using baseline and 12-month follow-up scans in

TABLE 1 Demographic information for the groups used in this analysis. Data is presented as mean ± standard error. One-way analysis of variances (ANOVAs) were used for group comparisons of age, education and cognition from which *P* values are shown. Significant comparisons are shown in bold.

	Aβ-			Group difference	
	Control	MCI	Aβ+	F	P
N (M/F)	31 (12/19)	20 (12/8)	40 (20/20)		
Age	70.5 ± 6.0	73.8 ± 6.6	76.8 ± 8.2	6.722	**0.002**
APOE ε4+	9	4	20	–	–
Education	16.2 ± 2.2	16.4 ± 2.7	15.6 ± 2.8	0.651	0.524
MOCA	25.2 ± 2.4	22.3 ± 3.7	22.4 ± 3.5	7.824	**$<10^{-3}$**
MMSE	29.0 ± 1.1	28.4 ± 1.8	27.6 ± 2.3	4.738	**0.011**
CDR global	0.0 ± 0.0	0.3 ± 0.2	0.4 ± 0.3	23.062	**$<10^{-3}$**
CDR SB	0.0 ± 0.0	0.9 ± 0.7	1.3 ± 1.5	12.422	**$<10^{-3}$**
ADAS13	8.5 ± 3.7	16.0 ± 5.3	16.0 ± 8.4	13.263	**$<10^{-3}$**
ADAS delayed recall	3.8 ± 2.1	2.7 ± 1.8	5.1 ± 2.6	11.590	**$<10^{-3}$**

the Aβ-control group. Thirteen control participants (nine female; mean age = 77.0 years; standard deviation of age = 7.2 years) had baseline and 12-month follow-up scans and the mean time between scans was 403 days (standard deviation = 49 days). Cortical susceptibility in the temporal lobe (ICC: 0.801; $P < 10^{-3}$), frontal lobe (ICC: 0.828; $P < 10^{-3}$), occipital lobe (ICC: 0.835; $P < 10^{-3}$) and parietal lobe (ICC: 0.855; $P < 10^{-3}$) showed excellent reproducibility. Interscan reproducibility for these ROIs is shown in Figure S1.

3.1.2 | Group differences in susceptibility

The effect of group (Aβ+, Aβ- MCI, Aβ- control) on susceptibility was assessed with separate ANCOVAs for each ROI (temporal lobe, hippocampus) with sex and age as a covariate. For the temporal lobe, no significant main effect of group ($P = 0.125$; $F = 2.137$) was observed. For the hippocampus, a significant main effect of group ($P = 0.039$; $F = 3.372$) revealed higher susceptibility in the Aβ+ group relative to the Aβ- control ($P = 0.011$) group. These results are summarized in Table 2.

3.1.3 | Group differences in tau-PET SUVR

The effect of group on tau-PET SUVR was assessed with separate ANCOVAs for each ROI, with sex, age and ROI susceptibility as covariates (Figures 2–3). For the temporal lobe, a significant main effect of group ($P = 0.008$; $F = 5.173$) revealed higher tau-PET SUVR in the Aβ + group relative to the Aβ- MCI and control groups (*Ps*<0.026), the latter of which did not differ from each other ($P = 0.459$). Age ($P = 0.080$; $F = 3.158$) and sex ($P = 0.827$; $F = 0.040$) were not a significant covariate in the model but tissue susceptibility ($P = 0.027$; $F = 5.107$) was a significant covariate in the model.

For the hippocampus, a significant main effect of group ($P = 0.010$; $F = 4.891$) similarly revealed higher tau-PET SUVR in the Aβ+ group relative to the Aβ- MCI ($P = 0.008$) and control ($P = 0.012$) groups, the latter of which did not differ from each other ($P = 0.573$). Age ($P = 0.034$; $F = 4.679$) and tissue susceptibility ($P = 0.034$; $F = 4.680$) were significant covariates in the model but sex was not a significant covariate ($P = 0.506$; $F = 0.447$).

3.1.4 | Group differences in tissue microstructure

The effect of the group on the microstructure was assessed with separate ANCOVAs for each ROI and diffusion parameter (FA, MD, fiso, ficvf), with sex and age as covariates (Figure 3). Tissue susceptibility was added as a covariate for FA and MD comparisons. For the temporal lobe, significant main effects of group were seen for FA ($P = 0.012$; $F = 4.638$), MD ($P = 0.021$; $F = 4.070$) and fiso ($P = 0.027$; $F = 3.780$), but not ficvf ($P = 0.301$; $F = 1.221$). A pairwise comparison of the marginal means revealed significantly lower temporal lobe FA ($P = 0.002$) and higher temporal lobe MD ($P = 0.006$) and fiso ($P = 0.011$) in the Aβ+ group relative to the control group. No other pairwise comparisons were significant (*Ps*>0.088). Age was a significant covariate in each

TABLE 2 Group differences for hippocampal and temporal lobe imaging metrics. Data is presented as mean ± standard deviation. One-way analysis of covariances (ANCOVAs) were used for group comparisons controlling for sex and age from, which *P* values are shown. Variables where susceptibility was controlled for are italicized. Significant comparisons are shown in bold.

	Aβ-			Group difference	
	Control	MCI	Aβ+	F	P
Temporal lobe susceptibility [ppm]	0.008 ± 0.005	0.009 ± 0.005	0.011 ± 0.006	2.137	0.125
Temporal lobe tau-PET SUVR	1.145 ± 0.072	1.117 ± 0.166	1.254 ± 0.244	4.967	**0.009**
Temporal lobe FA	0.191 ± 0.002	0.186 ± 0.002	0.184 ± 0.001	4.638	**0.012**
Temporal lobe MD [mm²/s]	$8.91 \times 10^{-4} \pm 1.2 \times 10^{-5}$	$9.25 \times 10^{-4} \pm 1.6 \times 10^{-5}$	$9.38 \times 10^{-4} \pm 1.1 \times 10^{-5}$	4.070	**0.021**
Temporal lobe fiso	0.271 ± 0.008	0.289 ± 0.011	0.302 ± 0.007	3.780	**0.027**
Temporal lobe ficvf	0.492 ± 0.004	0.482 ± 0.006	0.485 ± 0.004	1.221	0.301
Hippocampal susceptibility [ppm]	0.017 ± 0.010	0.020 ± 0.013	0.027 ± 0.019	3.372	**0.039**
Hippocampal tau-PET SUVR	1.383 ± 0.035	1.348 ± 0.050	1.514 ± 0.034	4.891	**0.010**
Hippocampal FA	0.146 ± 0.016	0.139 ± 0.010	0.133 ± 0.010	6.145	**0.003**
Hippocampal MD [mm²/s]	$8.85 \times 10^{-4} \pm 1.9 \times 10^{-5}$	$9.33 \times 10^{-4} \pm 2.5 \times 10^{-4}$	$9.96 \times 10^{-3} \pm 1.7 \times 10^{-4}$	9.003	**$<10^{-3}$**
Hippocampal fiso	0.243 ± 0.014	0.292 ± 0.019	0.328 ± 0.013	9.027	**$<10^{-3}$**
Hippocampal ficvf	0.435 ± 0.006	0.444 ± 0.008	0.442 ± 0.006	0.453	0.637

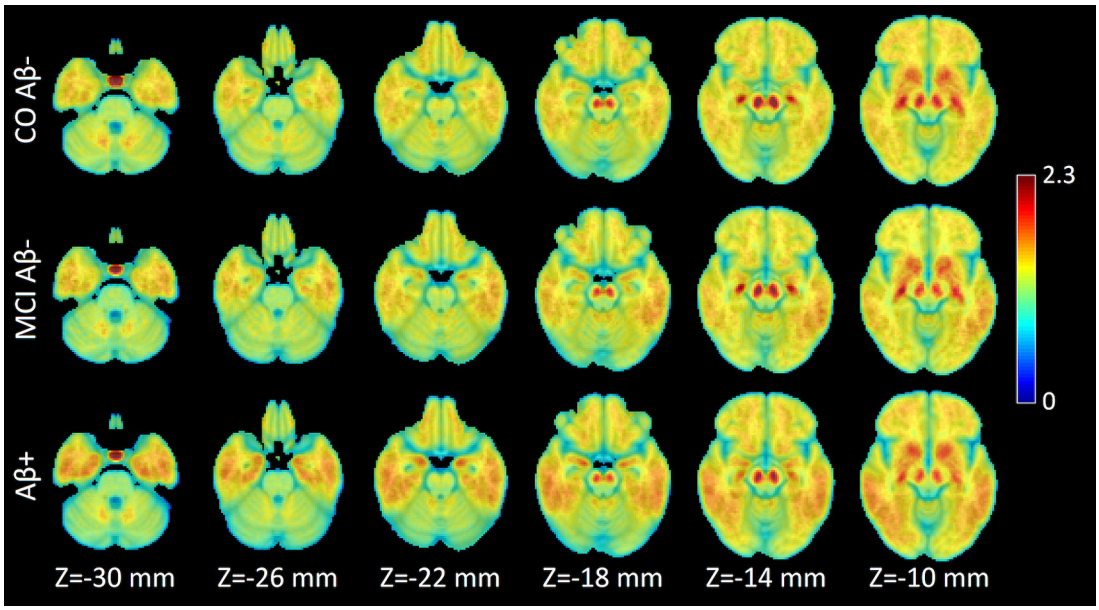

FIGURE 2 Comparison of tau-PET SUVR. Axial views of mean tau-PET SUVR in the Aβ- control (top row), Aβ- MCI (middle row) and Aβ+ (bottom row) groups. Elevated tau-PET SUVR is seen in the hippocampus and temporal lobe of the Aβ+ group relative to the Aβ- MCI and control groups.

model ($Ps<10^{-3}$; $Fs>11.315$) but sex, for all comparisons and tissue susceptibility, for comparisons with FA and MD, were not significant covariates ($Ps>0.175$; $Fs<1.874$).

For the hippocampus, significant main effects of the group were also seen for FA ($P = 0.003$; $F = 6.145$), MD ($P < 10^{-3}$; $F = 9.003$) and fiso ($P < 10^{-3}$; $F = 9.027$), but not ficvf ($P = 0.637$; $F = 0.453$). Pairwise comparison of

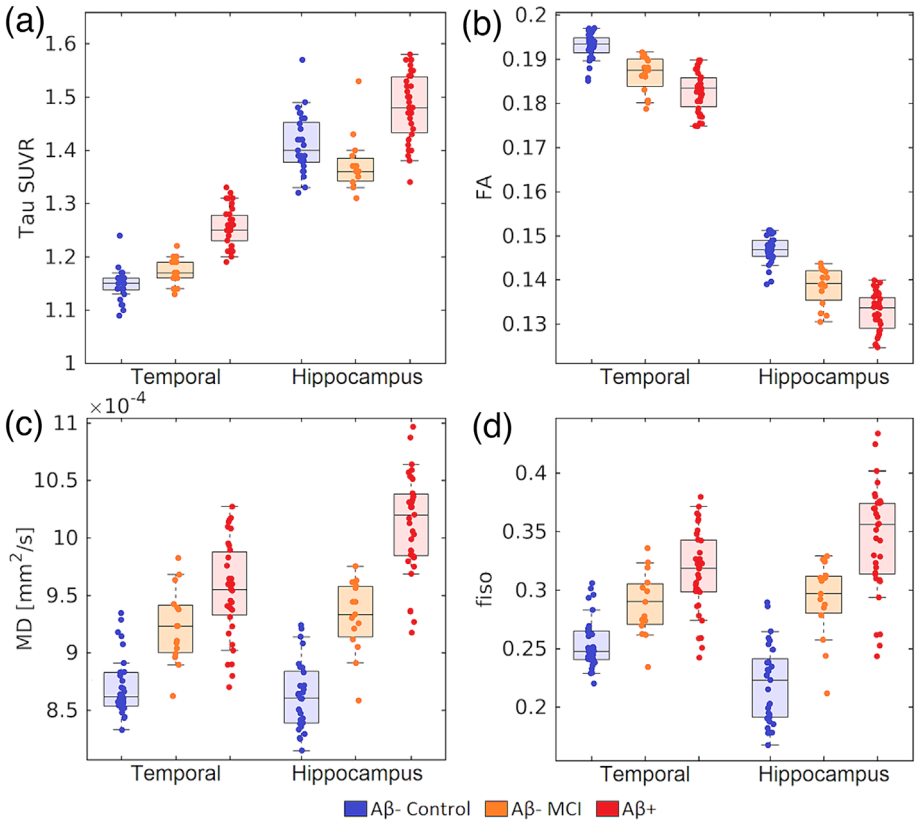

FIGURE 3 Group comparisons of tau SUVR (shown in A) and microstructural measures of FA (shown in B), MD (shown in C) and fiso (shown in D) in the temporal lobe and hippocampus ROIs. Significantly higher tau SUVR (A), MD (C) and fiso (D) and lower FA (B) were seen in the temporal lobe and hippocampus ROIs of the Aβ + group relative to the control group.

the marginal means revealed significantly lower hippocampal FA ($P = 0.002$) and higher hippocampal MD ($P < 10^{-3}$) and fiso ($P < 10^{-3}$) in the Aβ+ group relative to the control group. Higher hippocampal MD ($P = 0.047$) was seen in the Aβ+ group relative to the Aβ- MCI group. Significantly lower hippocampal FA ($P = 0.032$) and higher hippocampal fiso ($P = 0.041$) was also seen in the Aβ- MCI group relative to the control group. No other pairwise comparisons were significant (*Ps*>0.113). Age was a significant covariate in each model (*Ps*<0.004; *Fs*>8.662). Sex, for all variables, and tissue susceptibility, for FA and MD, were not significant covariates (*Ps*>0.095; *Fs*<2.856). These comparisons are summarized in Table 2.

3.1.5 | Relationships between tau-PET SUVR and susceptibility

A significant correlation between tau-PET SUVR and susceptibility was observed in the temporal lobe ($r = 0.279$; $P = 0.049$) and hippocampus ($r = 0.312$; $P = 0.044$) of the Aβ+ group. A significant correlation was seen in the hippocampus ($r = 0.597$; $P = 0.009$) but not in the temporal lobe ($r = 0.144$; $P = 0.149$) of the Aβ- MCI group. No association was observed between tau-PET SUVR and susceptibility in either ROI in the Aβ- control (temporal: $r = 0.273$; $P = 0.076$; hippocampus: $r = -0.009$; $P = 0.962$) groups. This relationship in the Aβ+ group, as well as their aforementioned elevated iron levels, may indicate iron-related off-target binding effects in tau-PET SUVR. The relationships between tau-PET SUVR and susceptibility in the hippocampus in the Aβ+ group are shown in Figure S2.

3.1.6 | Relationships between tau-PET SUVR and tissue microstructure

Separate multiple regressions were used to examine the impact of iron on the relationship between tau-PET SUVR and tissue microstructure (MD, FA, fiso, ficvf) before (model 1) and after (model 2) controlling for susceptibility in each ROI and each group. In the Aβ + group, tau-PET SUVR was a significant predictor of temporal lobe MD in model 1 ($\beta = 0.434$, $P = 0.020$) and in model 2 ($\beta = 0.464$, $P = 0.017$). Tau-PET SUVR was also a significant predictor of temporal lobe FA in model 1 ($\beta = -0.373$, $P = 0.046$) and ($\beta = -0.395$, $P = 0.038$). Tau-PET SUVR was not a significant predictor in either model for temporal lobe fiso (βs<0.367, *Ps*>0.066) or in either model for temporal lobe ficvf (βs<0.265, *Ps*>0.195). These relationships are summarized in Figure 4. Neither model was significant for hippocampal microstructure in

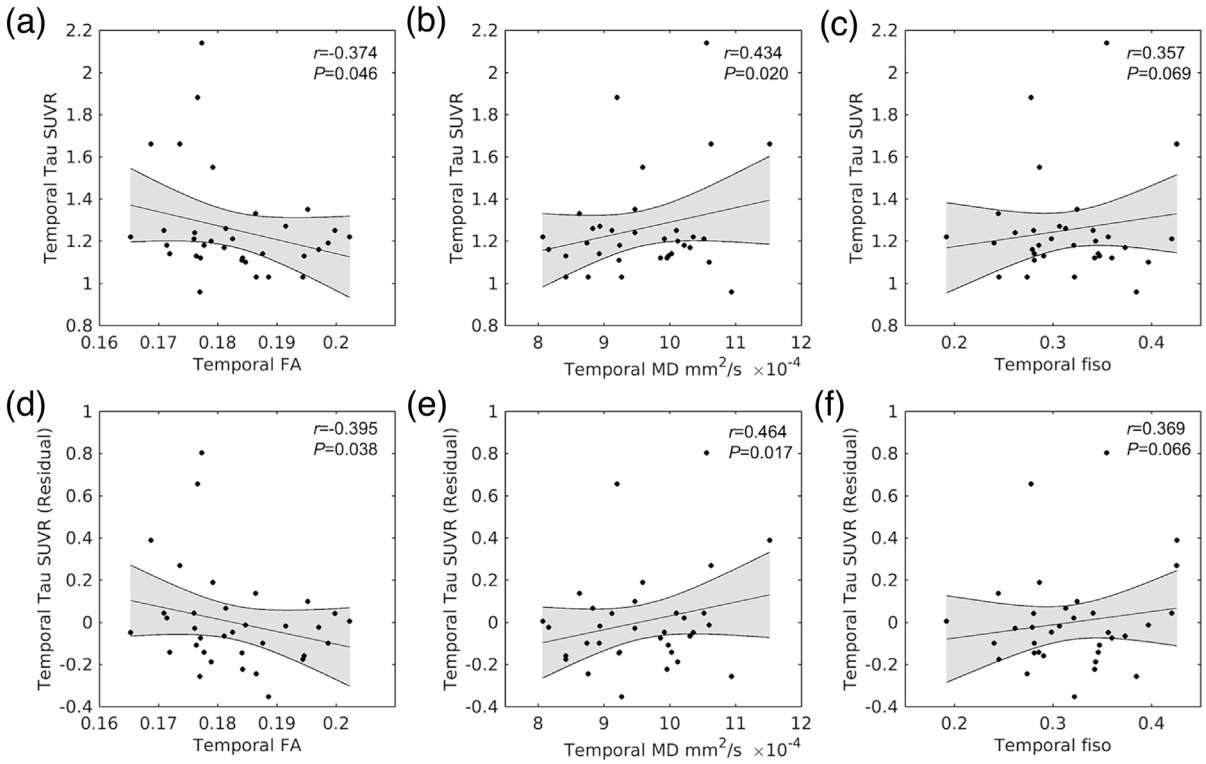

FIGURE 4 Correlations between mean temporal lobe tau-PET SUVR and temporal lobe microstructural measures of FA (shown in A), MD (shown in B) and fiso (shown in C) without controlling for temporal lobe susceptibility and the relationship between tau-PET SUVR and FA (shown in D), MD (shown E) and fiso (shown in F) after controlling for susceptibility in the Aβ+ group. Correlations remained significant before and after controlling for temporal lobe susceptibility.

the Aβ+ MCI group (*Ps*>0.423) or for microstructure in either ROI for the Aβ- MCI and Aβ- control groups (*Ps*>0.161).

3.1.7 | Relationships with cognition

The relationship between temporal lobe MD and cognition in the Aβ+ group is shown in Figure 5. Separate multiple regressions were used to examine the impact of iron on the relationship between tau-PET SUVR, iron-sensitive diffusion measures (MD, FA) and cognition (ADAS delayed word recall, ADAS11) before (model 1) and after (model 2) controlling for susceptibility in each ROI and each group. In the Aβ+ group, temporal lobe MD was a significant predictor of ADAS 11 in both models (model 1: $\beta = 0.378$, $P = 0.023$; model 2: $\beta = 0.363$, $P = 0.029$). Similarly, temporal lobe FA was a significant predictor of ADAS 11 in both models in the Aβ+ group (model 1: $\beta = 0.-374$, $P = 0.046$; model 2: $\beta = -0.395$, $P = 0.038$). In the hippocampus of the Aβ + group, hippocampal MD was a significant predictor of ADAS 11 and ADAS delayed recall (βs>0.382, *Ps*<0.020) but hippocampal FA was not a significant predictor of ADAS 11 and ADAS delayed recall (βs<−0.220, *Ps*>0.191). Tau-PET SUVR was not a significant predictor of cognition (ADAS delayed word recall or ADAS11) in either ROI of the Aβ+ group (βs<0.326, *Ps*>0.066). For the Aβ- MCI and Aβ- control groups, neither model was significant for either cognitive measure for each imaging measure in both ROIs (*Ps*>0.175).

4 | DISCUSSION

This study examines the relationship between tau deposition and both microstructural measures associated with neurodegeneration and cognition as a function of Aβ status, controlling for the off-target binding effects of iron. Compared to the Aβ- MCI and/or Aβ- control groups, the Aβ+ group had significantly higher tau pathology (tau-PET SUVR uptake) when controlling for iron, and microstructural degradation (increased MD, increased fiso, decreased FA) in the temporal lobe and hippocampus, as well as worse cognition. Tau pathology was related to iron and microstructure in the temporal lobe and hippocampus in the Aβ+ MCI group. Interestingly, correlations between tissue microstructure and

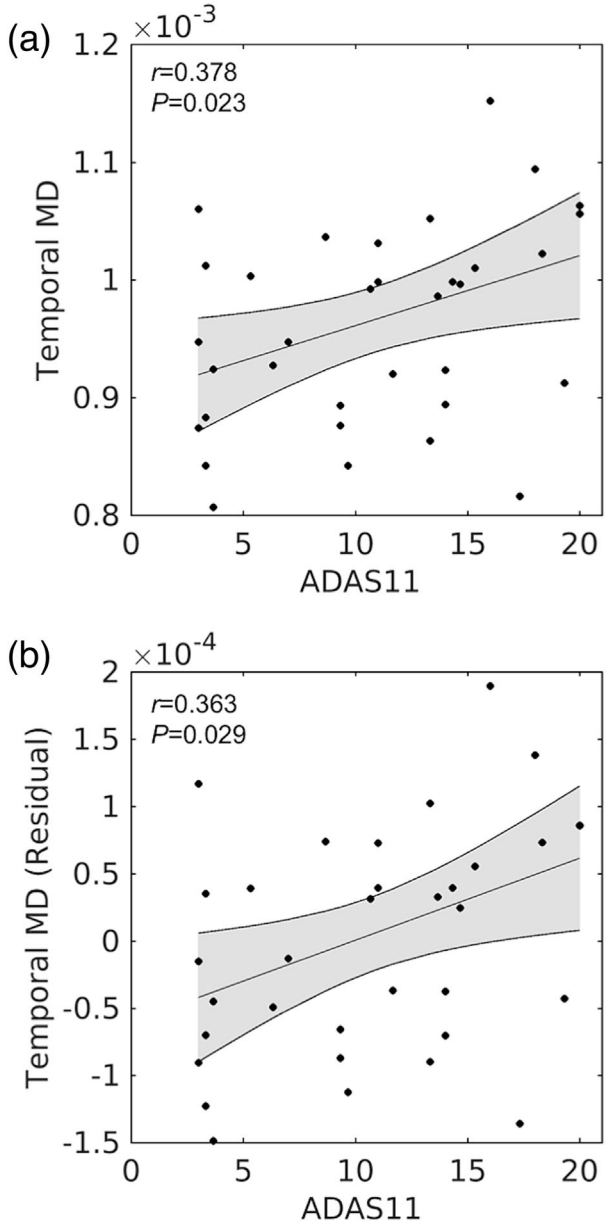

FIGURE 5 The relationship between temporal lobe tau SUVR and cognition in the Aβ+ group. Correlations between temporal lobe tau-PET SUVR and ADAS11 remained significant before (A) and after (B) controlling for susceptibility.

tau-PET SUVR remained unchanged when controlling for iron and suggest that iron-related off-target binding effects may not substantially contribute to tau-PET SUVR in the temporal lobe and hippocampus.

Postmortem studies of human and rodent tissue found iron is present in Aβ plaques (Connor et al., 1992; Meadowcroft et al., 2009) and Aβ plaques have been shown to exhibit elevated R_2* values (Meadowcroft et al., 2009). Consistent with this, imaging studies have reported elevated cortical iron levels in individuals with overt AD relative to controls (Ayton et al., 2020; Bulk et al., 2018; Damulina et al., 2020; van Bergen et al., 2016). In this study, higher susceptibility values were seen in the temporal lobe of Aβ+ participants relative to Aβ- participants. Our results suggest that temporal lobe iron deposition in AD may occur prior to the onset of dementia.

Tau deposition (Brecht et al., 2004; Tesseur et al., 2000; Wadhwani et al., 2019) has been reported in cognitively impaired individuals with AD. We similarly found higher iron and tau burden in the temporal lobe and hippocampus in the Aβ+ group relative to the Aβ- MCI and Aβ- control groups. Importantly, this result was seen using the ^{18}F-AV1451 radioligand and when controlling for iron with tissue susceptibility, as previous studies did not account for these possible off-target binding effects (Baek et al., 2020; Therriault et al., 2020). Moreover, relationships between cortical susceptibility and tau-PET SUVR have previously been observed in cognitively impaired individuals (Cogswell et al., 2021; Spotorno et al., 2020). In agreement with these studies, we found that iron content was associated with tau-PET SUVR in the temporal lobe and hippocampus in Aβ+ individuals as well as in the hippocampus of Aβ- MCI individuals. In contrast, no association was seen between susceptibility and tau-PET SUVR in either ROI in the Aβ- groups, which may be due to either low tau or iron deposition in these regions.

In AD, tau hyperphosphorylation is related to cortical thinning (das et al., 2018; la Joie et al., 2020; LaPoint et al., 2017) and cortical thinning should manifest in diffusion metrics as increased diffusivity or increases in the free water compartment in single-compartment or multi-compartment diffusion models, respectively. Prior imaging studies reported relationships between single-compartment DTI measures and tau-PET SUVR in the temporal lobe and hippocampus in AD (Carlson et al., 2021; Zhou & Bai, 2017). Interestingly, we observed a positive correlation between both temporal lobe MD and temporal lobe fiso with tau-PET SUVR. We extended this work by also examining multicompartment diffusion metrics (ficvf, fiso) and by controlling for susceptibility as both single-compartment diffusion measures (Langley et al., 2020; Syka et al., 2015) and tau-PET SUVR (Choi et al., 2018; Lockhart et al., 2017; Lowe et al., 2016; Marquié et al., 2017) are known to correlate with iron content. We found significant correlations between tau-PET SUVR and single-compartment diffusion measures (MD and FA) and fiso in the temporal lobe of the Aβ+ MCI group. These effects were significant in controlling for susceptibility and when susceptibility was not included in the model. This result suggests that relationships between diffusion and tau reported in prior studies (Carlson et al., 2021; Zhou & Bai, 2017) may be due to disease processes rather than to the influence of iron.

This study has several caveats. First, QSM is sensitive to iron (Langkammer et al., 2012) and is also sensitive to myelin (Liu et al., 2011). Our interest here was in grey matter regions (hippocampus, temporal lobe) with low myelin content and efforts were made to exclude white matter from our segmentations. Nonetheless, partial volume effects may include white matter and bias cortical susceptibility measurements. Second, iron deposition has been hypothesized to accelerate tau hyperphosphorylation (Yamamoto et al., 2002). Off-target binding of the ^{18}F-AV1451 radioligand to iron impedes investigation of the relationship between iron deposition and tau hyperphosphorylation.

In this work, tissue susceptibility was used to assess iron-related off-target binding effects with the ^{18}F-AV1451 radioligand in the hippocampus and temporal lobe in cognitively normal and impaired individuals that varied by Aβ status. We found significantly higher susceptibility, higher tau-PET SUVR uptake after controlling for iron and worse microstructure in the temporal lobe and hippocampus for the Aβ+ group relative to the Aβ- MCI and control groups. In the Aβ+ group, we found a significant correlation between susceptibility and tau-PET SUVR uptake in these regions, consistent with the notion that elevated iron in this group may contribute to off-target binding effects in tau-PET SUVR. We further found that controlling for susceptibility influenced correlations between tau-PET SUVR and diffusion metrics, but not cognitive performance. Specifically, relationships between tau-PET SUVR and microstructure were significant in the Aβ+ group before and after, controlling for iron, suggesting that microstructural correlations in this group may be due to AD pathology rather than off-target binding effects. In contrast, relationships between temporal lobe microstructural measures and cognitive performance were also only significant in the Aβ+ MCI group but did not differ when controlling for iron. Taken together, these results suggest that iron does not need to be accounted for in analyses of ^{18}F-AV1451 data in the cortex and hippocampus.

AUTHOR CONTRIBUTIONS

Jason Langley: Conceptualization; formal analysis; investigation; methodology; visualization; writing—original draft; writing—review and editing. **Ilana J. Bennett**: Conceptualization; Formal analysis; methodology; writing-review and editing. **Xiaoping Hu:** Conceptualization; methodology; writing-review and editing.

ACKNOWLEDGEMENTS

Data collection and sharing for this project was funded by the Alzheimer's Disease Neuroimaging Initiative (ADNI) (National Institutes of Health Grant U01 AG024904) and DOD ADNI (Department of Defense award number W81XWH-12-2-0012). ADNI is funded by the National Institute on Aging, the National Institute of Biomedical Imaging and Bioengineering, and through generous contributions from the following: AbbVie, Alzheimer's Association; Alzheimer's Drug Discovery Foundation; Araclon Biotech; BioClinica, Inc.; Biogen; Bristol-Myers Squibb Company; CereSpir, Inc.; Cogstate; Eisai Inc.; Elan Pharmaceuticals, Inc.; Eli Lilly and Company; EuroImmun; F. Hoffmann-La Roche Ltd and its affiliated company Genentech, Inc.; Fujirebio; GE Healthcare; IXICO Ltd.; Janssen Alzheimer Immunotherapy Research & Development, LLC.; Johnson & Johnson Pharmaceutical Research & Development LLC.; Lumosity; Lundbeck; Merck & Co., Inc.; Meso Scale Diagnostics, LLC.; NeuroRx Research; Neurotrack Technologies; Novartis Pharmaceuticals Corporation; Pfizer Inc.; Piramal Imaging; Servier; Takeda Pharmaceutical Company; and Transition Therapeutics. The Canadian Institutes of Health Research is providing funds to support ADNI clinical sites in Canada. Private sector contributions are facilitated by the Foundation fodar the National Institutes of Health (www.fnih.org). The grantee organization is the Northern California Institute for Research and Education, and the study is coordinated by the Alzheimer's Therapeutic Research Institute at the University of Southern California. ADNI data are disseminated by the Laboratory for Neuro Imaging at the University of Southern California. Ilana Bennett and Xiaoping Hu receive funding from National Institutes of Health Grant R01 AG072607.

CONFLICT OF INTEREST STATEMENT

None.

PEER REVIEW

The peer review history for this article is available at https://www.webofscience.com/api/gateway/wos/peer-review/10.1111/ejn.16362.

DATA AVAILABILITY STATEMENT

All data supporting these analyses are available through the Alzheimer's Disease Neuroimaging Initiative (ADNI) database (adni.loni.usc.edu).

ETHICS STATEMENTS

The authors report not conflicts of interest and all participants in the study gave written informed consent in accordance with local institutional review board (IRB) regulations.

ORCID

Jason Langley https://orcid.org/0000-0001-9412-1265
Ilana J. Bennett https://orcid.org/0000-0002-5330-4679
Xiaoping P. Hu https://orcid.org/0000-0001-7014-5983

REFERENCES

Albert, M. S., DeKosky, S. T., Dickson, D., Dubois, B., Feldman, H. H., Fox, N. C., Gamst, A., Holtzman, D. M., Jagust, W. J., Petersen, R. C., Snyder, P. J., Carrillo, M. C., Thies, B., & Phelps, C. H. (2011). The diagnosis of mild cognitive impairment due to Alzheimer's disease: Recommendations from the National Institute on Aging-Alzheimer's Association workgroups on diagnostic guidelines for Alzheimer's disease. *Alzheimers Dement*, *7*, 270–279. https://doi.org/10.1016/j.jalz.2011.03.008

Arnsten, A. F. T., Datta, D., Tredici, K. D., & Braak, H. (2021). Hypothesis: Tau pathology is an initiating factor in sporadic Alzheimer's disease. *Alzheimers Dement*, *17*, 115–124. https://doi.org/10.1002/alz.12192

Ayton, S., Faux, N. G., & Bush, A. I. (2015). Alzheimer's disease neuroimaging I., ferritin levels in the cerebrospinal fluid predict Alzheimer's disease outcomes and are regulated by APOE. *Nature Communications*, *6*, 6760. https://doi.org/10.1038/ncomms7760

Ayton, S., Wang, Y., Diouf, I., Schneider, J. A., Brockman, J., Morris, M. C., & Bush, A. I. (2020). Brain iron is associated with accelerated cognitive decline in people with Alzheimer pathology. *Molecular Psychiatry*, *25*, 2932–2941. https://doi.org/10.1038/s41380-019-0375-7

Baek, M. S., Cho, H., Lee, H. S., Lee, J. H., Ryu, Y. H., & Lyoo, C. H. (2020). Effect of APOE epsilon4 genotype on amyloid-beta and tau accumulation in Alzheimer's disease. *Alzheimer's Research & Therapy*, *12*, 140. https://doi.org/10.1186/s13195-020-00710-6

Beaulieu, C. (2002). The basis of anisotropic water diffusion in the nervous system—A technical review. *NMR in Biomedicine*, *15*, 435–455. https://doi.org/10.1002/nbm.782

Bejanin, A., Schonhaut, D. R., la Joie, R., Kramer, J. H., Baker, S. L., Sosa, N., Ayakta, N., Cantwell, A., Janabi, M., Lauriola, M., O'Neil, J. P., Gorno-Tempini, M. L., Miller, Z. A., Rosen, H. J., Miller, B. L., Jagust, W. J., & Rabinovici, G. D. (2017). Tau pathology and neurodegeneration contribute to cognitive impairment in Alzheimer's disease. *Brain*, *140*, 3286–3300. https://doi.org/10.1093/brain/awx243

Braak, H., Thal, D. R., Ghebremedhin, E., & Del Tredici, K. (2011). Stages of the pathologic process in Alzheimer disease: Age categories from 1 to 100 years. *Journal of Neuropathology and Experimental Neurology*, *70*, 960–969. https://doi.org/10.1097/NEN.0b013e318232a379

Brecht, W. J., Harris, F. M., Chang, S., Tesseur, I., Yu, G. Q., Xu, Q., Dee Fish, J., Wyss-Coray, T., Buttini, M., Mucke, L., Mahley, R. W., & Huang, Y. (2004). Neuron-specific apolipoprotein e4 proteolysis is associated with increased tau phosphorylation in brains of transgenic mice. *The Journal of Neuroscience*, *24*, 2527–2534. https://doi.org/10.1523/JNEUROSCI.4315-03.2004

Brookmeyer, R., Johnson, E., Ziegler-Graham, K., & Arrighi, H. M. (2007). Forecasting the global burden of Alzheimer's disease. *Alzheimers Dement*, *3*, 186–191. https://doi.org/10.1016/j.jalz.2007.04.381

Bulk, M., Abdelmoula, W. M., Nabuurs, R. J. A., van der Graaf, L. M., Mulders, C. W. H., Mulder, A. A., Jost, C. R., Koster, A. J., van Buchem, M. A., Natté, R., Dijkstra, J., & van der Weerd, L. (2018). Postmortem MRI and histology demonstrate differential iron accumulation and cortical myelin organization in early- and late-onset Alzheimer's disease. *Neurobiology of Aging*, *62*, 231–242. https://doi.org/10.1016/j.neurobiolaging.2017.10.017

Carlson, M. L., Toueg, T. N., Khalighi, M. M., Castillo, J., Shen, B., Azevedo, E. C., DiGiacomo, P., Mouchawar, N., Chau, G., Zaharchuk, G., James, M. L., Mormino, E. C., & Zeineh, M. M. (2021). Hippocampal subfield imaging and fractional anisotropy show parallel changes in Alzheimer's disease tau progression using simultaneous tau-PET/MRI at 3T. *Alzheimers Dement (Amst)*, *13*, e12218. https://doi.org/10.1002/dad2.12218

Chen Jingyun, Li, Y., Pirraglia, E., Okamura, N., Rusinek, H., de Leon, M. J., & de Leon, M. J. (2018). Quantitative evaluation of tau PET tracers (18)F-THK5351 and (18)F-AV-1451 in Alzheimer's disease with standardized uptake value peak-alignment (SUVP) normalization. *European Journal of Nuclear Medicine and Molecular Imaging*, *45*, 1596–1604. https://doi.org/10.1007/s00259-018-4040-1

Chételat, G., Villemagne, V. L., Villain, N., Jones, G., Ellis, K. A., Ames, D., Martins, R. N., Masters, C. L., Rowe, C. C., & AIBL Research Group. (2012). Accelerated cortical atrophy in cognitively normal elderly with high beta-amyloid deposition. *Neurology*, *78*, 477–484. https://doi.org/10.1212/WNL.0b013e318246d67a

Cho, H., Choi, J. Y., Hwang, M. S., Lee, J. H., Kim, Y. J., Lee, H. M., Lyoo, C. H., Ryu, Y. H., & Lee, M. S. (2016). Tau PET in Alzheimer disease and mild cognitive impairment. *Neurology*, *87*, 375–383. https://doi.org/10.1212/WNL.0000000000002892

Choi, J. Y., Cho, H., Ahn, S. J., Lee, J. H., Ryu, Y. H., Lee, M. S., & Lyoo, C. H. (2018). Off-target (18)F-AV-1451 binding in the basal ganglia correlates with age-related iron accumulation. *Journal of Nuclear Medicine*, *59*, 117–120. https://doi.org/10.2967/jnumed.117.195248

Cogswell, P. M., Wiste, H. J., Senjem, M. L., Gunter, J. L., Weigand, S. D., Schwarz, C. G., Arani, A., Therneau, T. M., Lowe, V. J., Knopman, D. S., Botha, H., Graff-Radford, J., Jones, D. T., Kantarci, K., Vemuri, P., Boeve, B. F., Mielke, M. M., Petersen, R. C., & Jack, C. R. Jr. (2021). Associations of quantitative susceptibility mapping with Alzheimer's disease clinical and imaging markers. *NeuroImage*, *224*, 117433. https://doi.org/10.1016/j.neuroimage.2020.117433

Connor, J. R., Snyder, B. S., Beard, J. L., Fine, R. E., & Mufson, E. J. (1992). Regional distribution of iron and iron-regulatory proteins in the brain in aging and Alzheimer's disease. *Journal of Neuroscience Research*, *31*, 327–335. https://doi.org/10.1002/jnr.490310214

Damulina, A., Pirpamer, L., Soellradl, M., Sackl, M., Tinauer, C., Hofer, E., Enzinger, C., Gesierich, B., Duering, M., Ropele, S., Schmidt, R., & Langkammer, C. (2020). Cross-sectional and longitudinal assessment of brain iron level in Alzheimer disease using 3-T MRI. *Radiology*, *296*, 619–626. https://doi.org/10.1148/radiol.2020192541

das, S., Xie, L., Wisse, L. E. M., Ittyerah, R., Tustison, N. J., Dickerson, B. C., Yushkevich, P. A., Wolk, D. A., & Alzheimer's Disease Neuroimaging Initiative. (2018). Longitudinal and cross-sectional structural magnetic resonance imaging correlates of AV-1451 uptake. *Neurobiology of Aging*, *66*, 49–58. https://doi.org/10.1016/j.neurobiolaging.2018.01.024

Doraiswamy, P. M., Sperling, R. A., Coleman, R. E., Johnson, K. A., Reiman, E. M., Davis, M. D., Grundman, M., Sabbagh, M. N., Sadowsky, C. H., Fleisher, A. S., Carpenter, A., Clark, C. M., Joshi, A. D., Mintun, M. A., Skovronsky, D. M., Pontecorvo, M. J., For the AV45-A11 Study Group, Duara, R., Sabbagh, M., … Sadowsky, C. H. (2012). Amyloid-beta assessed by florbetapir F 18 PET and 18-month cognitive decline: A multicenter study. *Neurology*, *79*, 1636–1644. https://doi.org/10.1212/WNL.0b013e3182661f74

Gómez-Isla, T., Hollister, R., West, H., Mui, S., Growdon, J. H., Petersen, R. C., Parisi, J. E., & Hyman, B. T. (1997). Neuronal loss correlates with but exceeds neurofibrillary tangles in Alzheimer's disease. *Annals of Neurology*, *41*, 17–24. https://doi.org/10.1002/ana.410410106

Gordon, B. A., McCullough, A., Mishra, S., Blazey, T. M., Su, Y., Christensen, J., Dincer, A., Jackson, K., Hornbeck, R. C., Morris, J. C., Ances, B. M., & Benzinger, T. L. S. (2018). Cross-sectional and longitudinal atrophy is preferentially associated with tau rather than amyloid beta positron emission tomography pathology. *Alzheimers Dement (Amst)*, *10*, 245–252. https://doi.org/10.1016/j.dadm.2018.02.003

Hardy, J., & Allsop, D. (1991). Amyloid deposition as the central event in the aetiology of Alzheimer's disease. *Trends in Pharmacological Sciences*, *12*, 383–388. https://doi.org/10.1016/0165-6147(91)90609-V

Hedden, T., Oh, H., Younger, A. P., & Patel, T. A. (2013). Meta-analysis of amyloid-cognition relations in cognitively normal older adults. *Neurology*, *80*, 1341–1348. https://doi.org/10.1212/WNL.0b013e31828ab35d

Iaccarino, L., Tammewar, G., Ayakta, N., Baker, S. L., Bejanin, A., Boxer, A. L., Gorno-Tempini, M. L., Janabi, M., Kramer, J. H., Lazaris, A., Lockhart, S. N., Miller, B. L., Miller, Z. A., O'Neil, J. P., Ossenkoppele, R., Rosen, H. J., Schonhaut, D. R., Jagust, W. J., & Rabinovici, G. D. (2018). Local and distant relationships between amyloid, tau and neurodegeneration in Alzheimer's disease. *NeuroImage: Clinical*, *17*, 452–464. https://doi.org/10.1016/j.nicl.2017.09.016

Jenkinson, M., Bannister, P., Brady, M., & Smith, S. (2002). Improved optimization for the robust and accurate linear registration and motion correction of brain images. *NeuroImage*, *17*, 825–841. https://doi.org/10.1006/nimg.2002.1132

Jenkinson, M., & Smith, S. (2001). A global optimisation method for robust affine registration of brain images. *Medical Image Analysis*, *5*, 143–156. https://doi.org/10.1016/S1361-8415(01)00036-6

Johnson, K. A., Schultz, A., Betensky, R. A., Becker, J. A., Sepulcre, J., Rentz, D., Mormino, E., Chhatwal, J., Amariglio, R., Papp, K., Marshall, G., Albers, M., Mauro, S., Pepin, L., Alverio, J., Judge, K., Philiossaint, M., Shoup, T., Yokell, D., … Sperling, R. (2016). Tau positron emission tomographic imaging in aging and early Alzheimer disease. *Annals of Neurology*, *79*, 110–119. https://doi.org/10.1002/ana.24546

Koivunen, J., Scheinin, N., Virta, J. R., Aalto, S., Vahlberg, T., Någren, K., Helin, S., Parkkola, R., Viitanen, M., & Rinne, J. O. (2011). Amyloid PET imaging in patients with mild cognitive impairment: A 2-year follow-up study. *Neurology*, *76*, 1085–1090. https://doi.org/10.1212/WNL.0b013e318212015e

la Joie, R., Visani, A. V., Baker, S. L., Brown, J. A., Bourakova, V., Cha, J., Chaudhary, K., Edwards, L., Iaccarino, L., Janabi, M., Lesman-Segev, O. H., Miller, Z. A., Perry, D. C., O'Neil, J. P., Pham, J., Rojas, J. C., Rosen, H. J., Seeley, W. W., Tsai, R. M., … Rabinovici, G. D. (2020). Prospective longitudinal atrophy in Alzheimer's disease correlates with the intensity and topography of baseline tau-PET. *Science Translational Medicine*, *12*, eaau7532. https://doi.org/10.1126/scitranslmed.aau5732

Labbe, C., Froment, J. C., Kennedy, A., Ashburner, J., & Cinotti, L. (1996). Positron emission tomography metabolic data corrected for cortical atrophy using magnetic resonance imaging. *Alzheimer Disease and Associated Disorders*, *10*, 141–170. https://doi.org/10.1097/00002093-199601030-00005

Landis, J. R., & Koch, G. G. (1977). The measurement of observer agreement for categorical data. *Biometrics*, *33*, 159–174. https://doi.org/10.2307/2529310

Langkammer, C., Schweser, F., Krebs, N., Deistung, A., Goessler, W., Scheurer, E., Sommer, K., Reishofer, G., Yen, K., Fazekas, F., Ropele, S., & Reichenbach, J. R. (2012). Quantitative susceptibility mapping (QSM) as a means to measure brain iron? A post mortem validation study. *NeuroImage*, *62*, 1593–1599. https://doi.org/10.1016/j.neuroimage.2012.05.049

Langley, J., Huddleston, D. E., & Hu, X. (2021). Nigral diffusivity, but not free water, correlates with iron content in Parkinson's disease. *Brain Communications*, *3*, fcab251. https://doi.org/10.1093/braincomms/fcab251

Langley, J., Hussain, S., Flores, J. J., Bennett, I. J., & Hu, X. (2020). Characterization of age-related microstructural changes in locus coeruleus and substantia nigra pars compacta. *Neurobiology of Aging*, *87*, 89–97. https://doi.org/10.1016/j.neurobiolaging.2019.11.016

LaPoint, M. R., Chhatwal, J. P., Sepulcre, J., Johnson, K. A., Sperling, R. A., & Schultz, A. P. (2017). The association between tau PET and retrospective cortical thinning in clinically normal elderly. *NeuroImage*, *157*, 612–622. https://doi.org/10.1016/j.neuroimage.2017.05.049

Lee, P., Kim, H. R., & Jeong, Y. (2020). Alzheimer's disease neuroimaging I. Detection of gray matter microstructural changes in Alzheimer's disease continuum using fiber orientation. *BMC Neurology*, *20*, 362. https://doi.org/10.1186/s12883-020-01939-2

Leuzy, A., Smith, R., Cullen, N. C., Strandberg, O., Vogel, J. W., Binette, A. P., Borroni, E., Janelidze, S., Ohlsson, T., Jögi, J., Ossenkoppele, R., Palmqvist, S., Mattsson-Carlgren, N., Klein, G., Stomrud, E., & Hansson, O. (2022). Biomarker-based prediction of longitudinal tau positron emission tomography in Alzheimer disease. *JAMA Neurology*, *79*, 149–158. https://doi.org/10.1001/jamaneurol.2021.4654

Li, W., Avram, A. V., Wu, B., Xiao, X., & Liu, C. (2014). Integrated Laplacian-based phase unwrapping and background phase removal for quantitative susceptibility mapping. *NMR in Biomedicine*, *27*, 219–227. https://doi.org/10.1002/nbm.3056

Li, W., Wang, N., Yu, F., Han, H., Cao, W., Romero, R., Tantiwongkosi, B., Duong, T. Q., & Liu, C. (2015). A method

for estimating and removing streaking artifacts in quantitative susceptibility mapping. *NeuroImage*, *108*, 111–122. https://doi.org/10.1016/j.neuroimage.2014.12.043

Li, W., Wu, B., & Liu, C. (2011). Quantitative susceptibility mapping of human brain reflects spatial variation in tissue composition. *NeuroImage*, *55*, 1645–1656. https://doi.org/10.1016/j.neuroimage.2010.11.088

Lim, Y. Y., Pietrzak, R. H., Ellis, K. A., Jaeger, J., Harrington, K., Ashwood, T., Szoeke, C., Martins, R. N., Bush, A. I., Masters, C. L., Rowe, C. C., Villemagne, V. L., Ames, D., Darby, D., & Maruff, P. (2013). Rapid decline in episodic memory in healthy older adults with high amyloid-beta. *Journal of Alzheimer's Disease*, *33*, 675–679. https://doi.org/10.3233/JAD-2012-121516

Liu, C., Li, W., Johnson, G. A., & Wu, B. (2011). High-field (9.4 T) MRI of brain dysmyelination by quantitative mapping of magnetic susceptibility. *NeuroImage*, *56*, 930–938. https://doi.org/10.1016/j.neuroimage.2011.02.024

Lockhart, S. N., Ayakta, N., Winer, J. R., la Joie, R., Rabinovici, G. D., & Jagust, W. J. (2017). Elevated (18)F-AV-1451 PET tracer uptake detected in incidental imaging findings. *Neurology*, *88*, 1095–1097. https://doi.org/10.1212/WNL.0000000000003724

Lowe, V. J., Curran, G., Fang, P., Liesinger, A. M., Josephs, K. A., Parisi, J. E., Kantarci, K., Boeve, B. F., Pandey, M. K., Bruinsma, T., Knopman, D. S., Jones, D. T., Petrucelli, L., Cook, C. N., Graff-Radford, N. R., Dickson, D. W., Petersen, R. C., Jack, C. R. Jr., & Murray, M. E. (2016). An autoradiographic evaluation of AV-1451 tau PET in dementia. *Acta Neuropathologica Communications*, *4*, 58. https://doi.org/10.1186/s40478-016-0315-6

Marquié, M., Verwer, E. E., Meltzer, A. C., Kim, S. J. W., Agüero, C., Gonzalez, J., Makaretz, S. J., Siao Tick Chong, M., Ramanan, P., Amaral, A. C., Normandin, M. D., Vanderburg, C. R., Gomperts, S. N., Johnson, K. A., Frosch, M. P., & Gómez-Isla, T. (2017). Lessons learned about [F-18]-AV-1451 off-target binding from an autopsy-confirmed Parkinson's case. *Acta Neuropathologica Communications*, *5*, 75. https://doi.org/10.1186/s40478-017-0482-0

Meadowcroft, M. D., Connor, J. R., Smith, M. B., & Yang, Q. X. (2009). MRI and histological analysis of beta-amyloid plaques in both human Alzheimer's disease and APP/PS1 transgenic mice. *Journal of Magnetic Resonance Imaging*, *29*, 997–1007. https://doi.org/10.1002/jmri.21731

Novikov, D. S., Reisert, M., & Kiselev, V. G. (2018). Effects of mesoscopic susceptibility and transverse relaxation on diffusion NMR. *Journal of Magnetic Resonance*, *293*, 134–144. https://doi.org/10.1016/j.jmr.2018.06.007

Ossenkoppele, R., Schonhaut, D. R., Schöll, M., Lockhart, S. N., Ayakta, N., Baker, S. L., O'Neil, J. P., Janabi, M., Lazaris, A., Cantwell, A., Vogel, J., Santos, M., Miller, Z. A., Bettcher, B. M., Vossel, K. A., Kramer, J. H., Gorno-Tempini, M. L., Miller, B. L., Jagust, W. J., & Rabinovici, G. D. (2016). Tau PET patterns mirror clinical and neuroanatomical variability in Alzheimer's disease. *Brain*, *139*, 1551–1567. https://doi.org/10.1093/brain/aww027

Ossenkoppele, R., Smith, R., Ohlsson, T., Strandberg, O., Mattsson, N., Insel, P. S., Palmqvist, S., & Hansson, O. (2019). Associations between tau, Abeta, and cortical thickness with cognition in Alzheimer disease. *Neurology*, *92*, e601–e612. https://doi.org/10.1212/WNL.0000000000006875

Pascoal, T. A., Benedet, A. L., Tudorascu, D. L., Therriault, J., Mathotaarachchi, S., Savard, M., Lussier, F. Z., Tissot, C., Chamoun, M., Kang, M. S., Stevenson, J., Massarweh, G., Guiot, M. C., Soucy, J. P., Gauthier, S., & Rosa-Neto, P. (2021). Longitudinal 18F-MK-6240 tau tangles accumulation follows Braak stages. *Brain*, *144*, 3517–3528. https://doi.org/10.1093/brain/awab248

Passamonti, L., Vázquez Rodríguez, P., Hong, Y. T., Allinson, K. S., Williamson, D., Borchert, R. J., Sami, S., Cope, T. E., Bevan-Jones, W. R., Jones, P. S., Arnold, R., Surendranathan, A., Mak, E., Su, L., Fryer, T. D., Aigbirhio, F. I., O'Brien, J. T., & Rowe, J. B. (2017). 18F-AV-1451 positron emission tomography in Alzheimer's disease and progressive supranuclear palsy. *Brain*, *140*, 781–791. https://doi.org/10.1093/brain/aww340

Sayre, L. M., Perry, G., Harris, P. L. R., Liu, Y., Schubert, K. A., & Smith, M. A. (2000). In situ oxidative catalysis by neurofibrillary tangles and senile plaques in Alzheimer's disease: A central role for bound transition metals. *Journal of Neurochemistry*, *74*, 270–279. https://doi.org/10.1046/j.1471-4159.2000.0740270.x

Schrag, M., Crofton, A., Zabel, M., Jiffry, A., Kirsch, D., Dickson, A., Mao, X. W., Vinters, H. V., Domaille, D. W., Chang, C. J., & Kirsch, W. (2011). Effect of cerebral amyloid angiopathy on brain iron, copper, and zinc in Alzheimer's disease. *Journal of Alzheimer's Disease*, *24*, 137–149. https://doi.org/10.3233/JAD-2010-101503

Selkoe, D. J. (1991). The molecular pathology of Alzheimer's disease. *Neuron*, *6*, 487–498. https://doi.org/10.1016/0896-6273(91)90052-2

Sintini, I., Schwarz, C. G., Martin, P. R., Graff-Radford, J., Machulda, M. M., Senjem, M. L., Reid, R. I., Spychalla, A. J., Drubach, D. A., Lowe, V. J., Jack, C. R. Jr., Josephs, K. A., & Whitwell, J. L. (2019). Regional multimodal relationships between tau, hypometabolism, atrophy, and fractional anisotropy in atypical Alzheimer's disease. *Human Brain Mapping*, *40*, 1618–1631. https://doi.org/10.1002/hbm.24473

Smith, S. M., Jenkinson, M., Woolrich, M. W., Beckmann, C. F., Behrens, T. E. J., Johansen-Berg, H., Bannister, P. R., de Luca, M., Drobnjak, I., Flitney, D. E., Niazy, R. K., Saunders, J., Vickers, J., Zhang, Y., de Stefano, N., Brady, J. M., & Matthews, P. M. (2004). Advances in functional and structural MR image analysis and implementation as FSL. *NeuroImage*, *23*(Suppl 1), S208–S219. https://doi.org/10.1016/j.neuroimage.2004.07.051

Spotorno, N., Acosta-Cabronero, J., Stomrud, E., Lampinen, B., Strandberg, O. T., van Westen, D., & Hansson, O. (2020). Relationship between cortical iron and tau aggregation in Alzheimer's disease. *Brain*, *143*, 1341–1349. https://doi.org/10.1093/brain/awaa089

Syka, M., Keller, J., Klempíř, J., Rulseh, A. M., Roth, J., Jech, R., Vorisek, I., & Vymazal, J. (2015). Correlation between relaxometry and diffusion tensor imaging in the globus pallidus of Huntington's disease patients. *PLoS ONE*, *10*, e0118907. https://doi.org/10.1371/journal.pone.0118907

Tesseur, I., van Dorpe, J., Spittaels, K., van den Haute, C., Moechars, D., & van Leuven, F. (2000). Expression of human apolipoprotein E4 in neurons causes hyperphosphorylation of

protein tau in the brains of transgenic mice. *The American Journal of Pathology*, *156*, 951–964. https://doi.org/10.1016/S0002-9440(10)64963-2

Therriault, J., Benedet, A. L., Pascoal, T. A., Mathotaarachchi, S., Chamoun, M., Savard, M., Thomas, E., Kang, M. S., Lussier, F., Tissot, C., Parsons, M., Qureshi, M. N. I., Vitali, P., Massarweh, G., Soucy, J. P., Rej, S., Saha-Chaudhuri, P., Gauthier, S., & Rosa-Neto, P. (2020). Association of apolipoprotein E epsilon4 with medial temporal tau independent of amyloid-beta. *JAMA Neurology*, *77*, 470–479. https://doi.org/10.1001/jamaneurol.2019.4421

Thomas, B. A., Cuplov, V., Bousse, A., Mendes, A., Thielemans, K., Hutton, B. F., & Erlandsson, K. (2016). PETPVC: A toolbox for performing partial volume correction techniques in positron emission tomography. *Physics in Medicine and Biology*, *61*, 7975–7993. https://doi.org/10.1088/0031-9155/61/22/7975

Thomas, B. A., Erlandsson, K., Modat, M., Thurfjell, L., Vandenberghe, R., Ourselin, S., & Hutton, B. F. (2011). The importance of appropriate partial volume correction for PET quantification in Alzheimer's disease. *European Journal of Nuclear Medicine and Molecular Imaging*, *38*, 1104–1119. https://doi.org/10.1007/s00259-011-1745-9

Torso, M., Bozzali, M., Zamboni, G., Jenkinson, M., Chance, S. A., & for the Alzheimers Disease Neuroimage Initiative. (2021). Detection of Alzheimer's disease using cortical diffusion tensor imaging. *Human Brain Mapping*, *42*, 967–977. https://doi.org/10.1002/hbm.25271

van Bergen, J. M., Li, X., Hua, J., Schreiner, S. J., Steininger, S. C., Quevenco, F. C., Wyss, M., Gietl, A. F., Treyer, V., Leh, S. E., Buck, F., Nitsch, R. M., Pruessmann, K. P., van Zijl, P. C. M., Hock, C., & Unschuld, P. G. (2016). Colocalization of cerebral iron with amyloid beta in mild cognitive impairment. *Scientific Reports*, *6*, 35514. https://doi.org/10.1038/srep35514

van Duijn, S., Bulk, M., van Duinen, S. G., Nabuurs, R. J. A., van Buchem, M. A., van der Weerd, L., & Natté, R. (2017). Cortical iron reflects severity of Alzheimer's disease. *Journal of Alzheimer's Disease*, *60*, 1533–1545. https://doi.org/10.3233/JAD-161143

van Rooden, S., Doan, N. T., Versluis, M. J., Goos, J. D. C., Webb, A. G., Oleksik, A. M., van der Flier, W. M., Scheltens, P., Barkhof, F., Weverling–Rynsburger, A. W. E., Blauw, G. J., Reiber, J. H. C., van Buchem, M. A., Milles, J., & van der Grond, J. (2015). 7T T(2)*-weighted magnetic resonance imaging reveals cortical phase differences between early- and late-onset Alzheimer's disease. *Neurobiology of Aging*, *36*, 20–26. https://doi.org/10.1016/j.neurobiolaging.2014.07.006

Wadhwani, A. R., Affaneh, A., Van Gulden, S., & Kessler, J. A. (2019). Neuronal apolipoprotein E4 increases cell death and phosphorylated tau release in Alzheimer disease. *Annals of Neurology*, *85*, 726–739. https://doi.org/10.1002/ana.25455

Whitwell, J. L., Graff-Radford, J., Tosakulwong, N., Weigand, S. D., Machulda, M., Senjem, M. L., Schwarz, C. G., Spychalla, A. J., Jones, D. T., Drubach, D. A., Knopman, D. S., Boeve, B. F., Ertekin-Taner, N., Petersen, R. C., Lowe, V. J., Jack, C. R. Jr., & Josephs, K. A. (2018). [(18) F]AV-1451 clustering of entorhinal and cortical uptake in Alzheimer's disease. *Annals of Neurology*, *83*, 248–257. https://doi.org/10.1002/ana.25142

Woolrich, M. W., Jbabdi, S., Patenaude, B., Chappell, M., Makni, S., Behrens, T., Beckmann, C., Jenkinson, M., & Smith, S. M. (2009). Bayesian analysis of neuroimaging data in FSL. *NeuroImage*, *45*, S173–S186. https://doi.org/10.1016/j.neuroimage.2008.10.055

Xia, C., Makaretz, S. J., Caso, C., McGinnis, S., Gomperts, S. N., Sepulcre, J., Gomez-Isla, T., Hyman, B. T., Schultz, A., Vasdev, N., Johnson, K. A., & Dickerson, B. C. (2017). Association of in vivo [18F]AV-1451 tau PET imaging results with cortical atrophy and symptoms in typical and atypical Alzheimer disease. *JAMA Neurology*, *74*, 427–436. https://doi.org/10.1001/jamaneurol.2016.5755

Yamamoto, A., Shin, R. W., Hasegawa, K., Naiki, H., Sato, H., Yoshimasu, F., & Kitamoto, T. (2002). Iron (III) induces aggregation of hyperphosphorylated tau and its reduction to iron (II) reverses the aggregation: Implications in the formation of neurofibrillary tangles of Alzheimer's disease. *Journal of Neurochemistry*, *82*, 1137–1147. https://doi.org/10.1046/j.1471-4159.2002.t01-1-01061.x

Zhang, D., Snyder, A. Z., Shimony, J. S., Fox, M. D., & Raichle, M. E. (2010). Noninvasive functional and structural connectivity mapping of the human thalamocortical system. *Cerebral Cortex*, *20*, 1187–1194. https://doi.org/10.1093/cercor/bhp182

Zhang, H., Schneider, T., Wheeler-Kingshott, C. A., & Alexander, D. C. (2012). NODDI: Practical in vivo neurite orientation dispersion and density imaging of the human brain. *NeuroImage*, *61*, 1000–1016. https://doi.org/10.1016/j.neuroimage.2012.03.072

Zhong, J., Kennan, R. P., & Gore, J. C. (1991). Effects of susceptibility variations on NMR measurements of diffusion. *Journal of Magnetic Resonance*, *95*, 267–280.

Zhou, Y., & Bai, B. (2017). Tau and PET/MRI imaging biomarkers for detecting and diagnosing early dementia. *Jacobs Journal of Medical Diagnosis and Medical Imaging*, *2*, 017.

SUPPORTING INFORMATION

Additional supporting information can be found online in the Supporting Information section at the end of this article.

How to cite this article: Langley, J., Bennett, I. J., Hu, X. P., & for the Alzheimer's Disease Neuroimaging Initiative (2024). Examining iron-related off-target binding effects of ^{18}F-AV1451 PET in the cortex of Aβ+ individuals. *European Journal of Neuroscience*, 1–15. https://doi.org/10.1111/ejn.16362